Stochastic analysis of moisture plume dynamics of a field injection experiment

Ming Ye

Desert Research Institute, University and Community College System of Nevada, Las Vegas, Nevada, USA

Raziuddin Khaleel

Fluor Government Group, Richland, Washington, USA

Tian-Chyi J. Yeh

Department of Hydrology and Water Resources, University of Arizona, Tucson, Arizona, USA

Received 14 October 2004; accepted 13 January 2005; published 16 March 2005.

[1] A vadose zone field injection experiment was conducted in the summer of 2000 at the Hanford Site, Washington. The unique moisture content (θ) database is used to identify the lithology at the field site and to interpret, visualize, and quantify the spatiotemporal evolution of the three-dimensional (3-D) moisture plume created by the injection experiment. We conducted a hierarchical geostatistical analysis to examine the large-scale geologic structure for the entire field site and then investigated small-scale features within different layers. Afterward, variogram analysis was applied to the θ field measured for seven different days during the injection experiment. Temporal variations of sills and ranges are related to the observed moisture plume dynamics. A visualization of the 3-D moisture plume evolution illustrates effects of media heterogeneity. Statistics of changes in moisture content as a function of distance reveal large variance near the wetting front; the coefficient of variation increases with decreasing mean. These findings support the gradient- and mean-dependent variability in the moisture content distribution as reported by existing stochastic theories. Spatial moment analysis is also conducted to quantify the rate and direction of movement of the plume mass center and its spatial spreading. The ratio of horizontal to vertical spreading at varying moisture contents suggests moisture-dependent anisotropy in effective unsaturated hydraulic conductivity, confirming existing stochastic theories. However, the principal directions of the spatial moments are found to vary as the moisture plume evolves through local heterogeneity, a feature that has not been recognized in the theories.

Citation: Ye, M., R. Khaleel, and T.-C. J. Yeh (2005), Stochastic analysis of moisture plume dynamics of a field injection experiment, *Water Resour. Res.*, *41*, W03013, doi:10.1029/2004WR003735.

1. Introduction

[2] Knowledge of natural heterogeneity in geologic media leads to a better understanding and prediction of hydrological processes in subsurface environment. Effects of heterogeneity on vadose zone flow and transport have been reported for a number of field observations [*Trautwein et al.*, 1983; *Routson et al.*, 1979; *Price et al.*, 1979; *Crosby et al.*, 1968, 1971; *Prill*, 1977; *Knoll and Nelson*, 1962; *Palmquist and Johnson*, 1962]. As concluded in these studies, lateral movement of water and solutes is usually significant if the medium is stratified, the initial moisture content is low, the size of the application area is small relative to the size of the unsaturated zone, and the application rate is small [*Gelhar et al.*, 1985]. These conclusions were qualitative but they did provide the motivation and basis for subsequent theoretical work by Gelhar and his colleagues using a stochastic framework [e.g., *Yeh et al.*, 1985a, 1985b, 1985c; *Mantoglou and Gelhar*, 1987; *Ababou*, 1988; *Polmann et al.*, 1991]. By treating unsaturated zone hydraulic properties as a stochastic process, the theoretical work led to the development of stochastic methods for estimating effective hydraulic properties and quantifying uncertainty in predictions. Several new findings also emerged including moisture-dependent anisotropy in unsaturated hydraulic conductivity, hysteresis in effective properties, and the moisture-dependent variability of vadose zone processes [*Yeh et al.*, 1985a, 1985b, 1985c; *Mantoglou and Gelhar*, 1987].

[3] A number of large-scale vadose zone experiments have been conducted over the past two decades [*Sisson and Lu*, 1984; *Yeh et al.*, 1986; *Greenholtz et al.*, 1988; *Wierenga et al.*, 1991a, 1991b; *Rudolph et al.*, 1996]. Applications of stochastic methods to field problems however have been hindered by the need for a large number of measurements of hydraulic properties at small scales. These measurements are needed to accurately estimate their spatial statistics as required by stochastic methods [*Holt et al.*, 2002]. Cost and time constraints often prohibited collection

0043-1397/05/2004WR003735$09.00

of an extensive set of field measurements. As a result, attempts at evaluating stochastic theories for a large-scale vadose zone experiment [*Wierenga et al.*, 1991a, 1991b], for example, by *Polmann et al.* [1991] resulted in mixed success. In addition, the nature of stochastic theory and multiscale heterogeneity within the vadose zone call for assessment of the theory in a variety of geologic settings.

[4] *Ward et al.* [2000] and *Gee and Ward* [2001] recently conducted water and tracer injection experiments at a field site that was originally envisioned and designed by *Sisson and Lu* [1984]. The site is located within the U. S. Department of Energy Hanford Site in southeastern Washington, and hereafter is referred to as the S&L site. The injection experiments were conducted over a period of 2 months during the summer of 2000. Using neutron probes, Gee and Ward collected the initial and postinjection moisture contents (θ) for 32 wells and 43 depths over an area of 15 m $\times$ 15 m.

[5] Such an extensive and dense data set provides a unique opportunity that was not available in the past to quantify dynamics of moisture movement within the vadose zone. *Ward et al.* [2000], for example, illustrated the multidimensional distribution of θ at the S&L site. Variogram analysis of the initial moisture content measurements for the *Sisson and Lu* [1984] injection experiment was conducted by *Rockhold et al.* [1999]; a hole effect was reported for the resulting vertical variogram. *Gee and Ward* [2001] evaluated spatial moments up to second order, mean velocity in x, y, and z directions, cumulative travel distance, and path directions. These analyses illustrate the temporal variation of three-dimensional moisture content distribution and the effect of layering on the movement of injected water.

[6] Different from the preceding studies, our paper examines multiscale heterogeneous moisture field and relates the geostatistical finding to geological properties at the field site. We study the temporal evolution of the spatial statistics of the moisture plume before, during, and after injection, which is important for mapping soil moisture distributions over large areas. Our analysis also investigates several important findings of the stochastic theories such as (1) moisture content variability increases when the soil becomes less saturated, (2) the head variance is the largest near a wetting front, and (3) anisotropy in effective unsaturated hydraulic conductivity is moisture-dependent. More importantly, we analyze the principal directions of the moisture plume as it migrates and show how the directional changes are influenced by the local heterogeneity, a fact that is ignored in all previous theoretical work and application of geostatistical analyses. We expect that results of our work will provide new insight on evaluation of moisture plume dynamics in similar geological media.

2. Field Site and Injection Experiments

2.1. Site Description

[7] The climate of the Hanford Site is considered semiarid with an average annual precipitation of 16 cm. Nearly half the precipitation falls during November through February. Geologically, the upper portion of the field site was formed during catastrophic glacial flooding. Flood sediments were deposited when ice dams in western Montana and northern Idaho breached and massive volumes of water spilled across eastern and central Washington. A thick sequence of sediments was deposited by several episodes of Pleistocene flooding, the last major flood sequence dating about 13,000 years before present. These sediments are known as the Hanford formation, which is about 60 m deep at the S&L site. The sediments consist principally of sand with interstitial silt and silt beds that are interpreted as lenses [*Last and Caldwell*, 2001; *Last et al.*, 2001]. The depth to the water table is in excess of 90 m.

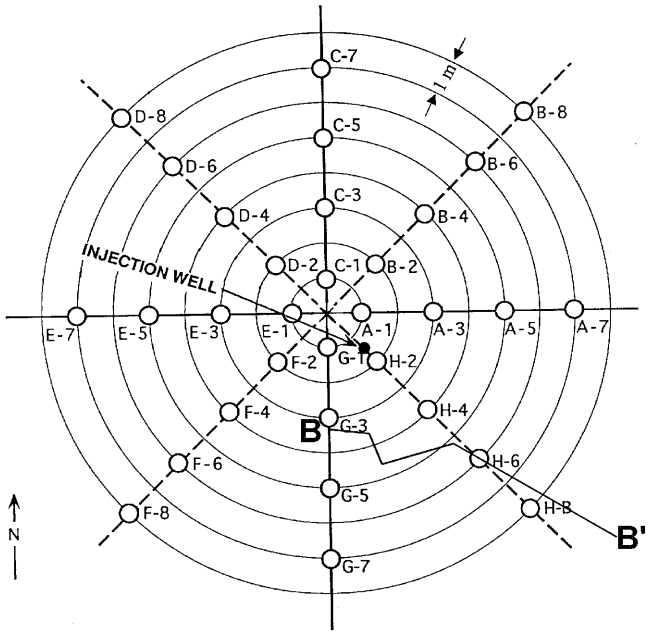

Figure 1. Plan view of the *Sisson and Lu* [1984] injection test site and well numbering scheme [after *Gee and Ward*, 2001]. The distance between neighboring circles is 1 m, as indicated in the top right corner. The lithostratigraphic cross section along B–B′ is shown in Figure 2.

2.2. The 1980 Experiments and Previous Work

[8] The S&L site (Figure 1) was used in late 1980 to conduct an infiltration experiment [*Sisson and Lu*, 1984]. A total of 45,000 L of liquid (in 11 increments) was injected at the central well at a depth of 4.7 m over a period of 133 days. The entire experiment was conducted within 20 m (below ground surface), well within the Hanford formation, and well above the water table. The initial moisture content field as well as the moisture content (θ) following successive injections was to be measured at 30-cm increments up to a depth of 18 m at the 32 radially arranged cased boreholes (Figure 1). Note that the radial distance between two adjacent circles in Figure 1 is 1 m. The largest radial distance between the center and the outermost observation well is thus 8 m. The 1980 θ database was not as frequent and dense as the 2000 database; the latter was used in this work.

[9] Several lithostratigraphic cross sections of the injection site are available from *Last et al.* [2001]. Figure 2 shows a lithostratigraphic cross section (B–B′ in Figure 1) through the southeastern portion of the injection site. While the cross section shows that the site mainly consists of sandy deposits, the presence of a distinctly larger fraction of

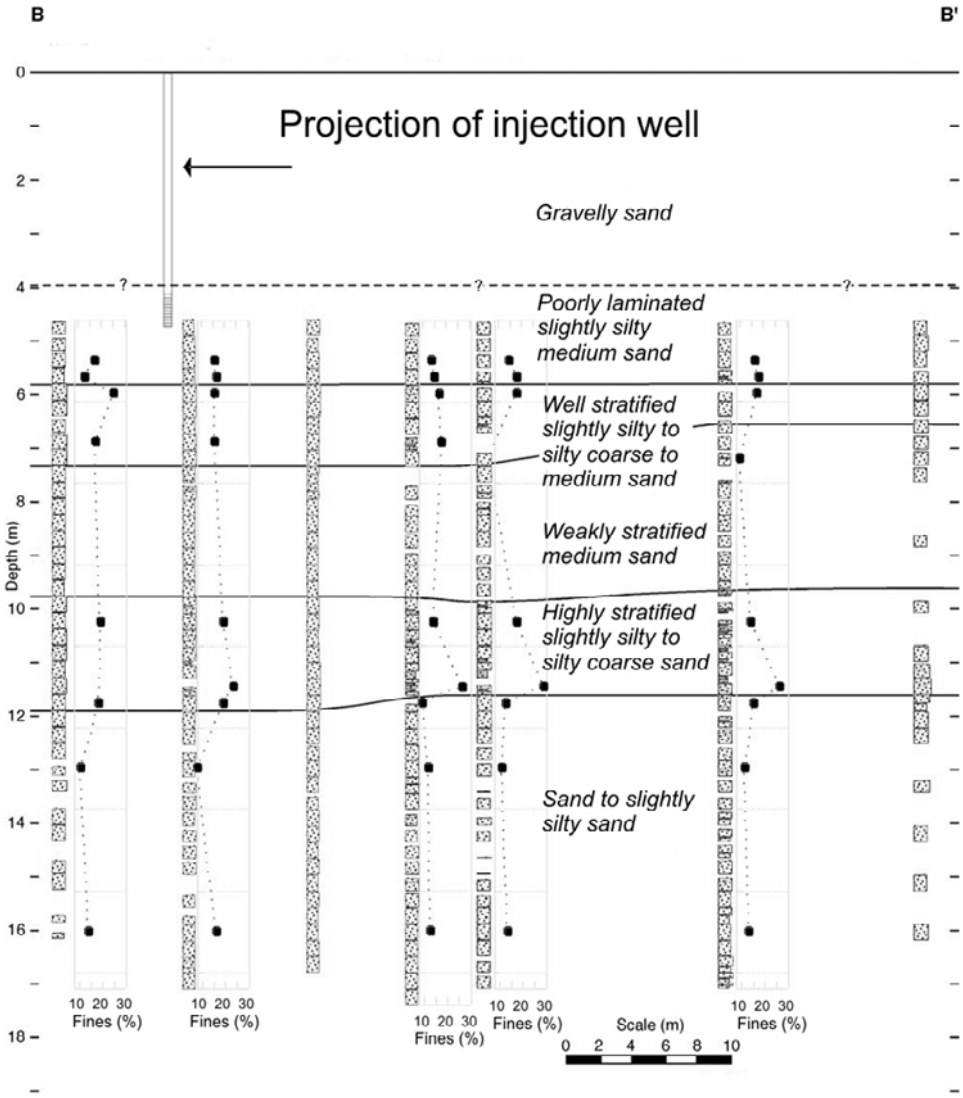

Figure 2. Lithostratigraphic cross section through the southeastern portion of the injection site [after *Last et al.*, 2001]. The location of cross section B–B′ is shown in Figure 1.

fine sediments in the middle two layers is noticeable. In addition, well-developed laminations exist within layers. Particle size distributions (PSD) of 15 samples at the S&L site are available from *Khaleel and Freeman* [1995] and *Khaleel et al.* [1995]. The fitted van Genuchten-Mualem [*Mualem*, 1976; *van Genuchten*, 1980] characteristic curves based on laboratory measurements of moisture retention, saturated and unsaturated conductivity for 15 repacked samples at the S&L site are included in our companion paper [*Yeh et al.*, 2005]. These data illustrate the variability in physical and hydraulic properties at the field site.

[10] Several investigators analyzed, with mixed success, effects of heterogeneity on the 1980 moisture plume using numerical modeling [*Sisson and Lu*, 1984; *Lu and Khaleel*, 1993; *Smoot*, 1995], geostatistical analyses [*Fayer et al.*, 1995; *Smoot*, 1995], and conditional simulation techniques [*Rockhold et al.*, 1999]. Sisson and Lu, for example, found a relatively good agreement between the observed and simulated moisture content history at locations close to the injection point but a significant bias in θ values at locations away from the injection point. Also, based on the assumption of a uniform and isotropic model, the modeling predicted a much deeper penetration of the moisture profile than what actually occurred in the field.

2.3. The 2000 Injection Experiments

[11] The S&L site was used for another infiltration test in 2000 [*Gee and Ward*, 2001]. Water content distribution was measured on 5 May 2000 at the 32 radially arranged cased boreholes. These measurements are referred to as initial moisture content (θ_i) in this and the companion paper. Injections began on 1 June and 4000 L of water were metered into a new injection point (near well H-2 in Figure 1) 5-m below the land surface over a 6-hour period. Similarly, 4000 L of water were injected in each subsequent injection on 8, 15, 22, and 28 June. During the injection period, neutron logging in 32 wells took place within a day following each of the first four injections (i.e., 2, 9, 16, and 23 June). A wildfire burned close to the test site and prevented immediate logging of the θ distribution for the fifth injection on 28 June. Three additional readings of the 32 wells were subsequently completed on 7, 17, and

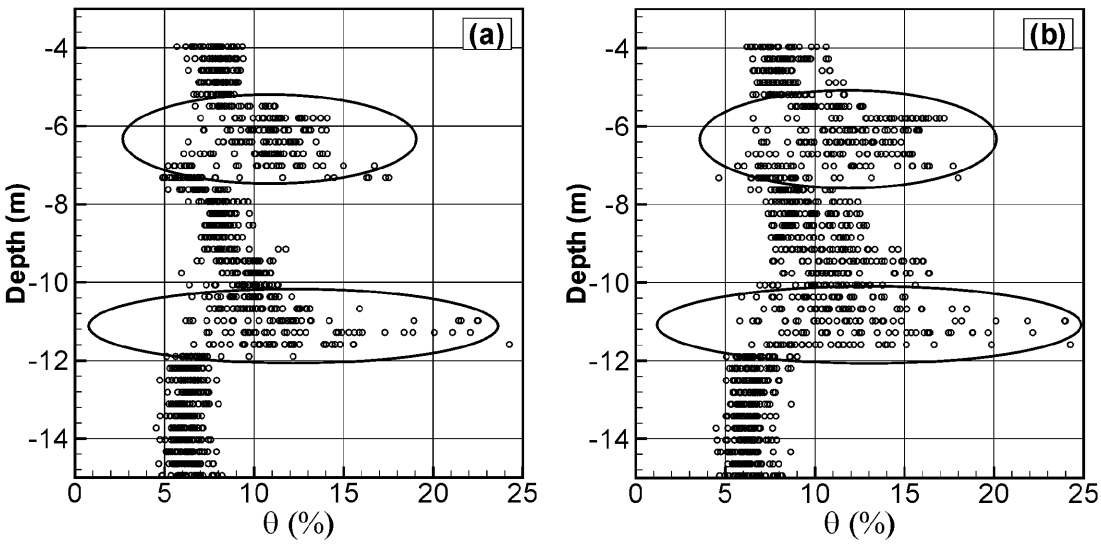

Figure 3. Moisture content (vol %) profiles measured on (a) 5 May 2000 and (b) 31 July 2000.

31 July. During each neutron logging, water contents were monitored at 0.305 m depth intervals starting from a depth of 3.97 m and continuing to a depth of 16.78 m, resulting in a total of 1344 measurements for the eight observation days over a 2-month period.

[12] The neutron probe used for the 2000 measurements was a Campbell Pacific Nuclear (CPN) neutron hydroprobe (Model 503 DR, serial number H33115140). The probe, slightly less than 5 cm in diameter, was lowered into the 15-cm diameter steel-cased access tubes (32 in number). Measurements were recorded by first lowering the probe to the bottom of the well of interest after which counts were accumulated over a 15-sec interval at 30-cm depth increments while withdrawing the probe from the well [*Ward et al.*, 2000]. The calibration function was obtained by regressing moisture content on 15-sec count times using a power function:

$$\theta = aN^b \tag{1}$$

where N = 15-sec neutron count, a = 4.18E-10 and b = 2.3225. The measurement volume of the neutron probe varies with θ, but for a soil with specified θ, about 95% of the measured slow neutrons are from a sphere of radius r (cm) [*Olgaard*, 1965]:

$$r = 100/(1.4 + \theta). \tag{2}$$

For θ measurements at the S&L site, r ranges from about 60 to 70 cm. Further details on the neutron probe calibration are given by *Ward et al.* [2000].

3. Hierarchical Analysis of Initial Moisture Content Distribution

[13] All the θ values collected on 5 May (initial) and 31 July (last observation) are plotted as a function of depth in Figures 3a and 3b, respectively, showing five distinct zones of low and high θ values. The five-zone pattern is similar to that found in the 1980 θ_i measurements. The consistency in these θ_i patterns over the 20-year time interval suggests that the 5 May θ_i distribution is under a state of natural equilibrium, with larger θ values associated with fine-textured materials and smaller values with coarse-textured materials. Since this interpretation of the θ_i pattern is in general agreement with the geologic cross section (Figure 2), we classified the site geology into five sediment layers. A bottom layer of coarse-textured sediments (∼3 m thick) is overlain by a layer of fine-textured sediments (∼2 m thick). Another layer of coarse-textured sediments (∼3 m thick) appears at a depth of about 10 m and is overlain by a layer of fine-textured sediments (∼2 m thick). Finally, a layer of coarse-textured sediments appears at a depth of about 5 m. These layers are assumed to be perfectly stratified. Table 1 summarizes the layer boundaries and statistics (mean, standard deviation, and coefficient of skewness) of θ_i and θ for each layer observed during the experiment. According to Table 1, the initial moisture content within each layer has different statistical properties and thus the θ_i distribution over the entire domain can be considered as a nonstationary process if ergodicity is assumed [*Priestley*, 1981].

[14] The apparent correspondence between the θ_i distribution and the geologic cross section prompted us to use the θ_i distribution as a means for describing geology at the S&L site. Geostatistical analysis of the θ_i distribution thus can yield a quantitative description of the three-dimensional geologic fabric (structure) at the field site. A hierarchical approach [e.g., *Barrash and Clemo*, 2002] is adopted for this purpose. First, we assess the sampling domain-level geologic structure by evaluating omnidirectional and directional variograms of θ_i. Then, separating θ_i measurements according to the identified layers, we investigate the layer-level structure by examining omnidirectional and directional variograms of θ_i for each layer.

3.1. Domain-Level Spatial Variability

[15] The omnidirectional experimental variogram (Figure 4) of the θ_i for the entire sampling domain appears to reach a stable sill and suggests an exponential variogram. On the other hand, the vertical experimental variogram (Figure 4) reveals a hole effect [*Isaaks and Srivastava*,

Table 1. Statistics of the Moisture Content (Volumetric) Distribution for Each Layer and the Entire Sampling Domain

	Layer 1	Layer 2	Layer 3	Layer 4	Layer 5	All Layers
Depth, m	−15∼−11.7	−9.9∼−11.7	−6.9∼−9.9	−5.4∼−6.9	−4.0∼−5.4	−4.0∼−11.7
Number of measurements	352	192	320	160	160	1184
5 May 2000						
Mean, %	6.29	11.12	8.49	10.41	7.93	8.46
Standard deviation, %	0.72	3.28	1.92	1.86	0.73	2.55
Skewness	−0.09	1.70	1.71	−0.13	−0.46	1.77
2 June 2000						
Mean, %	6.29	11.01	8.83	12.54	8.51	8.89
Standard deviation, %	0.71	3.27	2.07	3.74	2.00	3.16
Skewness	1.14	1.48	1.71	0.43	2.85	1.61
9 June 2000						
Mean, %	6.26	11.00	9.55	13.11	8.57	9.16
Standard deviation, %	0.67	3.26	3.06	3.92	2.11	3.50
Skewness	0.21	1.35	1.62	0.16	2.69	1.43
16 June 2000						
Mean, %	6.33	11.16	10.34	13.23	8.61	9.44
Standard deviation, %	0.77	3.27	3.60	3.99	2.25	3.72
Skewness	2.25	1.45	1.21	0.16	2.68	1.31
23 June 2000						
Mean, %	6.34	11.42	10.66	13.53	8.69	9.62
Standard deviation, %	0.71	3.30	3.65	3.90	2.35	3.80
Skewness	0.39	1.05	1.03	−0.048	2.59	1.16
7 July 2000						
Mean, %	6.29	11.83	10.11	12.66	8.42	9.49
Standard deviation, %	0.70	3.68	2.66	2.97	1.51	3.45
Skewness	0.20	1.00	1.12	−0.16	1.73	1.02
17 July 2000						
Mean, %	6.34	11.82	10.23	12.33	8.34	9.36
Standard deviation, %	0.70	3.57	2.58	2.72	1.33	3.23
Skewness	0.51	1.05	0.80	−0.10	1.05	1.06
31 July 2000						
Mean, %	6.37	11.78	10.01	12.05	8.21	8.21
Standard deviation, %	0.78	3.50	2.35	2.58	1.14	1.14
Skewness	0.63	1.17	0.88	−0.12	0.91	0.91

1989, p. 156] with a double-hump feature. The double hump of the vertical variogram implies a cyclicity in the θ_i field and, in turn, the presence of a cyclic sequence of coarse and fine sediments or irregular layers (strata) [*Pyrcz and Deutsch*, 2003] as revealed in the θ_i profiles (Figure 3) and the geologic cross section (Figure 2). The cyclicity occurs about every 3.5 m, which is corroborated by the average thickness of the layers at the field site. The horizontal variogram increases with lag without reaching a sill within the maximum lag distance of the sampling domain, implying a correlation scale in the horizontal direction that is greater than the domain's horizontal dimension (16 m). Such a correlation scale is supported by the relatively continuous bedding observed in the geologic cross section.

[16] The vertical variogram (Figure 4) is larger than the horizontal variogram, implying zonal anisotropy [*Wackernagel*, 1995]. A similar behavior was also observed by *Barrash and Clemo* [2002] for porosity data at the Boise Hydrogeophysical Site, Idaho. The zonal anisotropy can be attributed to the way the variograms are computed and the presence of nearly perfectly stratified bedding at the site. Specifically, only data pairs along the vertical direction are used in calculating the vertical variogram while only hor-

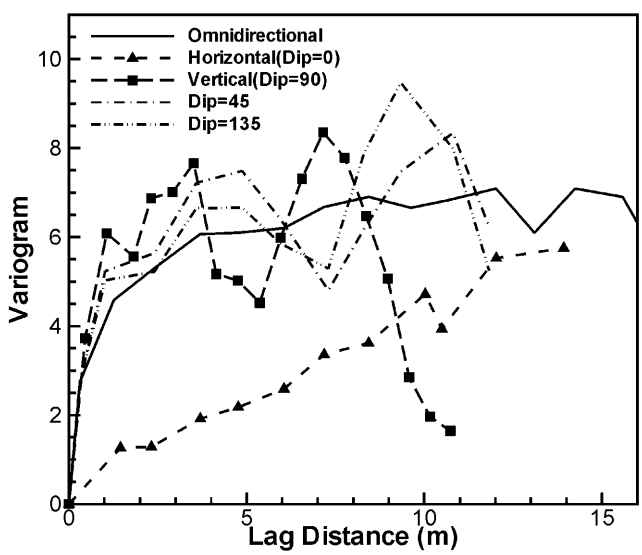

Figure 4. Omnidirectional and directional variograms of initial moisture content measurements for the entire sampling domain.

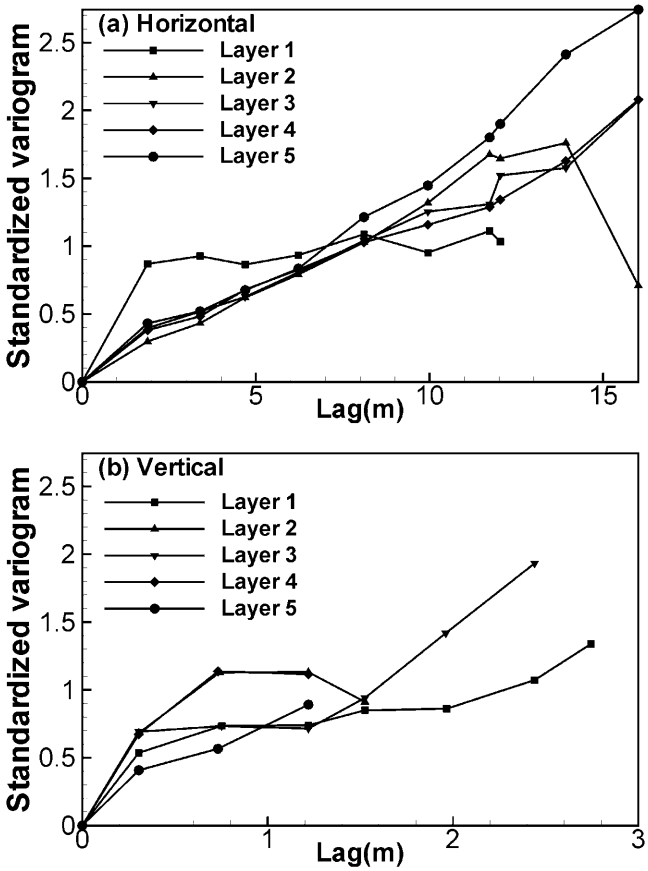

Figure 5. (a) Horizontal and (b) vertical variograms of initial θ within each of five layers.

izontal data pairs are considered in the horizontal variogram estimation. For the vertical variogram, data pairs more likely cross different geologic boundaries. As θ_i in the fine-textured layers is larger than θ_i in the coarse-textured layers, θ_i differences for the data pairs crossing the boundary are expected to be large. In contrast, horizontal variogram analysis only considers data pairs within either the coarse- or fine-textured layer, and θ_i differences for the data pair within the same layer are likely to be small. Hence a greater sill value of the vertical variogram than the horizontal is probable. Directional variograms corresponding to dip angles of 45° (dipping at an angle of 45° from horizontal) and 135° (dipping at an angle of 135° from horizontal) are plotted in Figure 4 as well. Since the data pair used include θ_i measurements from different layers, these directional variograms are larger than the horizontal variogram and have magnitudes similar to the vertical variogram. In comparison with the vertical variogram, a shifting of peaks in these variograms is noticeable, possibly associated with the dip angle. Overall, the θ_i measurements and, in turn, the geologic structure can be considered as isotropic in the horizontal direction, despite the fact that the horizontal variogram for the northeast direction increases faster than for the southwest direction (not shown here).

3.2. Layer-Level Spatial Variability

[17] Layer-level spatial variability of the θ_i measurements is first analyzed by evaluating its omnidirectional sample variograms. All sample variograms appear to increase with lag without reaching any sill within the maximum lag distance of the sampling domain (not shown here). This is also true for the directional sample variograms (except for layer 1) evaluated along horizontal directions (Figure 5a), suggesting a correlation scale in the horizontal direction that may be greater than the horizontal dimension (16 m) of the sampling domain. The vertical variograms (Figure 5b), on the other hand, appear to stabilize at lag distances that are of the same order and are either equal to or smaller than the sampling interval (0.305 m). Thus the vertical correlation scale of the θ_i field is smaller than the average layer thickness (3.5 m). This conclusion is consistent with the presence of fine-scale laminations in different layers [*Last et al.*, 2001]. In general, although the θ_i measurements within different layers have similar horizontal and vertical spatial correlation lengths, they have different means and variances (Table 1). Note that the uniform thickness assumption embedded in our classification of the five layers may have inevitably included materials from coarse-textured layers into fine-textured layers. This assumption thus may have had some effects on our results (such as the increase in the variogram for layers 3 and 5 in Figure 5).

4. Moisture Plume Dynamics

[18] The aim of this section is to quantify changes in the statistical structure of the θ distribution over the entire domain during the injection experiments. Our analysis of moisture plume dynamics evaluates the θ field for each observation day without removing the mean of each layer. The statistics of the θ field for the entire sampling domain are listed in Table 1, based on 8 days of data collected before, during and after injections. Note that the skewness (Table 1) persisted throughout the injection experiment.

4.1. Variogram Analyses

[19] The directional sample variograms were calculated for the θ_i and θ observed for the seven sampling days (during injection and redistribution). However, only the vertical ones are shown in Figure 6. All the vertical sample variograms exhibit a typical double-hump feature. Overall, during injections (2–23 June), variograms increase and the hump at small lag diminishes gradually. During redistribution (i.e., 7–31 July), the hump at the small lag appears gradually and the variogram returns toward that of θ_i. In contrast, all of the horizontal variograms (not shown here) show a continuous increase with lag during the injection experiments. The disappearance and reappearance of the double-hump feature can be related to the layered structure of the sediments and, as explained later in section 4.2, to the dynamics of movement of the injected water.

[20] As discussed in section 3.1, the difference in horizontal and vertical variogram magnitudes simply indicates that the horizontal correlation scale of the lithology is longer than the horizontal sampling domain. Had the horizontal sampling domain been many times the horizontal correlation scale such that it encompassed the same variability as in the vertical, the horizontal variogram would have reached the same sill as the vertical (i.e., geometric anisotropy). In theory, the variance of a stochastic process must be a scalar quantity [*Gelhar*, 1993].

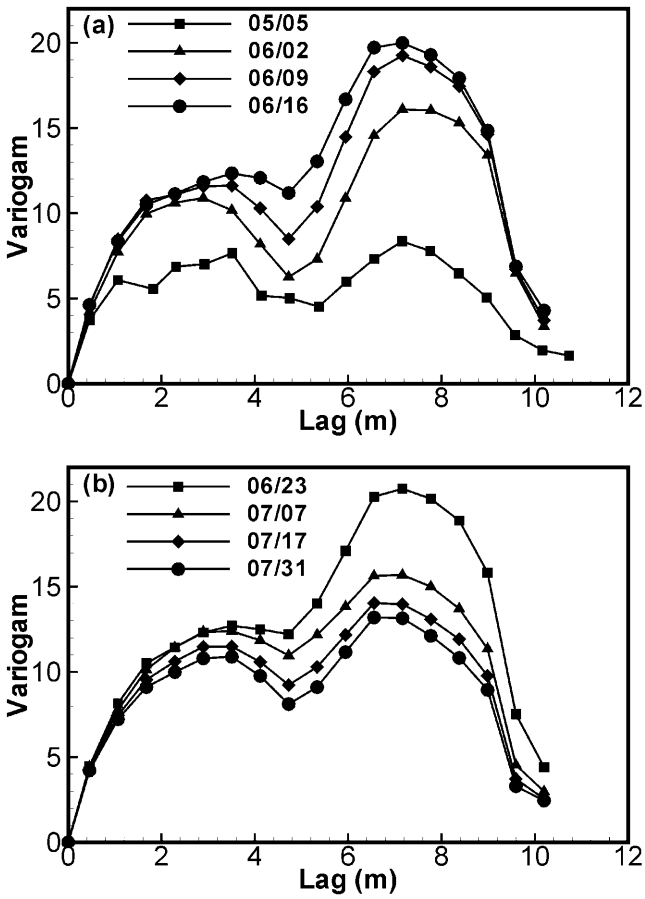

Figure 6. Vertical variograms of moisture contents on different days of the injection experiment. Read 5/05 as 5 May.

[21] The sample horizontal and vertical variograms were fitted to an exponential variogram model [*Deutsch and Journel*, 1998, p. 25]

$$\gamma(h) = c\left[1 - \exp\left(-\frac{3h}{a}\right)\right] \tag{3}$$

where c is the sill and a is the effective range, at which the variogram attains a constant value of about 0.95 c. When fitting vertical variogram parameters using a spreadsheet, we assign more weight to the fitting for small lags, since in the subsequent kriging analysis, data closer to the kriging point receives more weight than the distal points. In addition, we assume that the theoretical variogram is isotropic in the horizontal direction and their principal directions remain the same.

[22] Sills, horizontal range, and vertical range of the fitted theoretical variograms are shown in Figure 7 as function of days after the first injection. The sill values increase with the start of the injection experiments and decrease during the last three sampling days (7, 17, and 31 July) following the last injection on 28 June. The increase in the sill during the injection period is attributed to the creation of a region of higher θ than the antecedent ambient θ due to water injections. After the last injection event, the injected water redistributed and dispersed for a long period of time; the θ distribution thus became less variable overall, which resulted in the decrease in the sill value after 7 July.

[23] According to Figure 7, the horizontal ranges decrease first and then increase after 7 July while the vertical ranges increase first and then decrease. The presence of a less uniformly distributed θ field in the horizontal direction helps explain the decrease of horizontal ranges during the injections. The uninterrupted redistribution after the last injection led to the disappearance of the wet region and the increase in horizontal ranges after 7 July.

[24] Unlike the horizontal ranges, the vertical ranges increase during injections and decrease during the uninterrupted redistribution. The increase, which results in an enhanced spatial continuity of θ in the vertical direction, is attributed to the vertical movement of the injected water. The increase in the vertical continuity also explains the disappearance of the cyclic characteristic of the θ_i distribution. On the other hand, the uninterrupted lateral spreading of water after the last injection allowed the θ distribution to gradually approach the initial condition with its cyclic characteristic.

4.2. Visualization of Moisture Dynamics

[25] Using the theoretical variograms described in section 4.1 and a three-dimensional (3-D) ordinary kriging routine in GSLIB [*Deutsch and Journel*, 1998], the θ measurements for 32 wells and 43 depths for each observation period are projected onto a 3-D domain of size 15 m × 15 m × 12 m. The center of the top plane of the domain is set to be the same as that of the layout of the observation wells in Figure 1. The domain is discretized into 100,000 uniform elements of size 0.3 m × 0.3 m × 0.3 m to provide enough resolution for visualization and to reflect the measurement scale of the neutron probe. The kriged θ at the center of each element is assumed to represent θ for the entire element. Figure 8a illustrates the spatial distribution of initial θ on 5 May 2000.

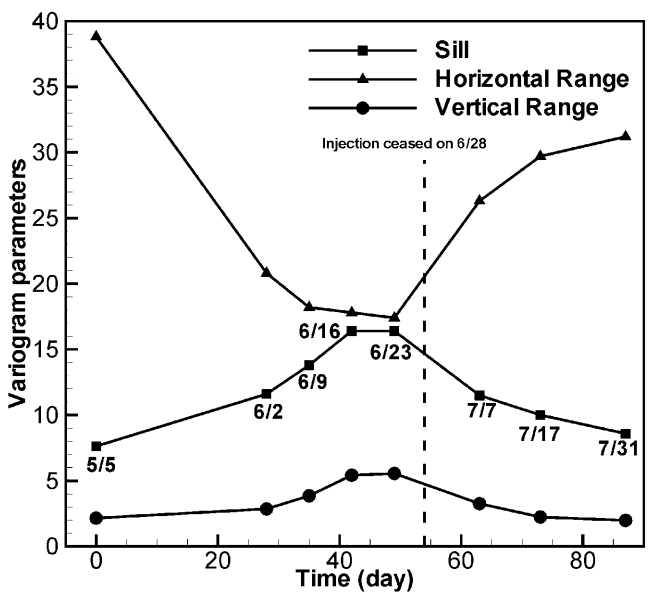

Figure 7. Variation of sills and horizontal and vertical ranges during the injection experiments.

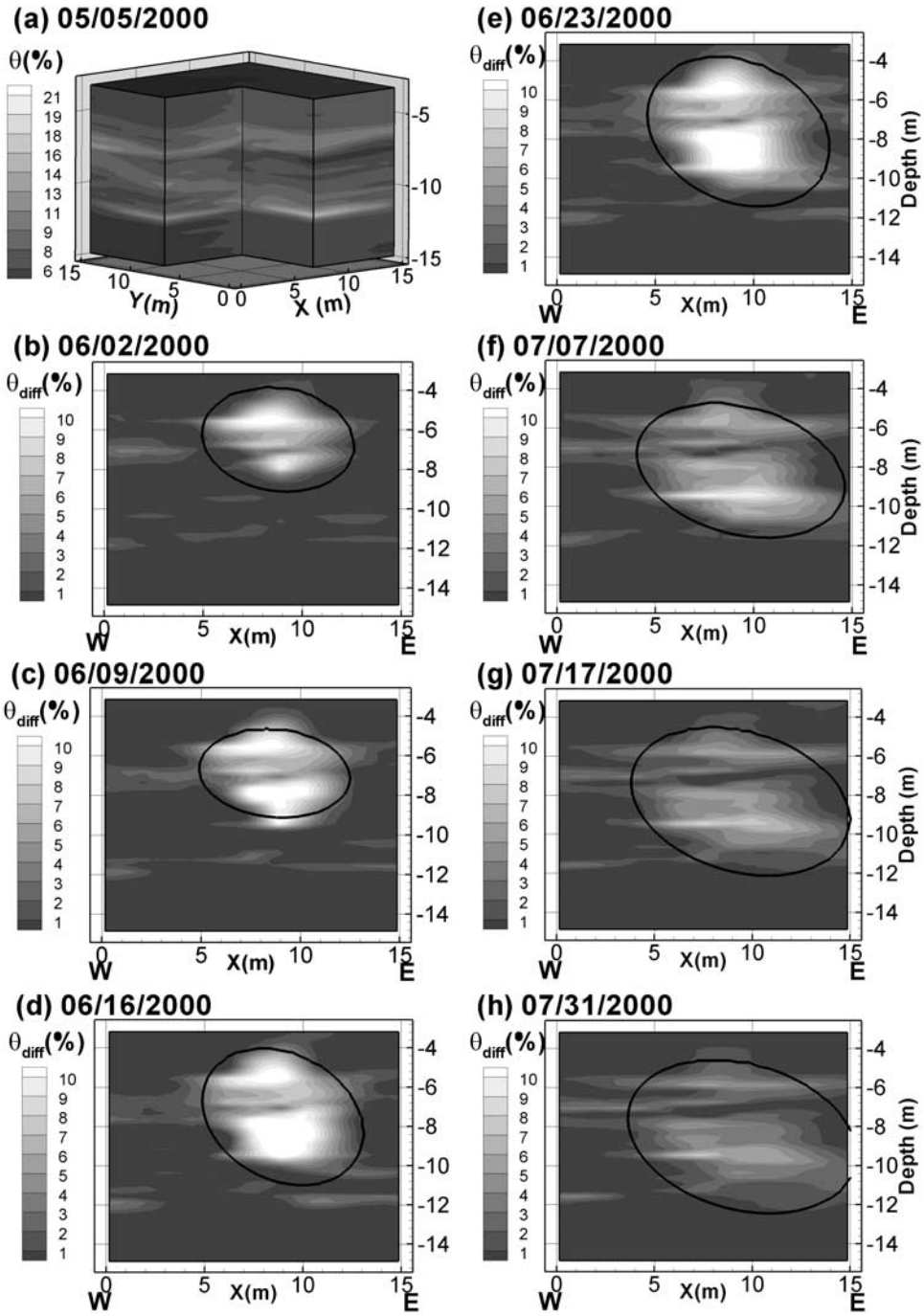

Figure 8. (a) Initial moisture content on 5 May and (b–h) east-west trending cross-sectional views of moisture content differences along the plane passing through the injection well. See color version of this figure at back of this issue.

[26] The moisture content differences (θ_{diff}) between the kriged θ for each observation day and the kriged initial θ are used to illustrate the dynamics of the moisture plume. Two-dimensional contours of θ_{diff} distribution in the east-west vertical plane passing through the injection well are illustrated in Figure 8. The ellipses in Figure 8 are cross sections of the ellipsoids estimated based on second spatial moments of θ_{diff} described in section 5.

[27] As shown in Figure 8, the injected water first encountered the top of the fine-textured layer at a depth of about 5 m. Some water accumulated above the layer, while some entered the layer and spread out laterally. Upon exceeding the air-entry pressure head of the underlying coarse-textured layer between depths of 7 and 10 m, the water penetrated the interface between the two layers. Once the water entered the coarse-textured layer, it moved vertically at a rate greater than the rate at which it was entering from the layer above, resulting in a change in the θ distribution. The lateral spread of θ in the coarse-textured material, however, was limited due to its small capillary effect [*Yeh et al.*, 2005]. The successive injections created a zone of persistently high θ in the fine-

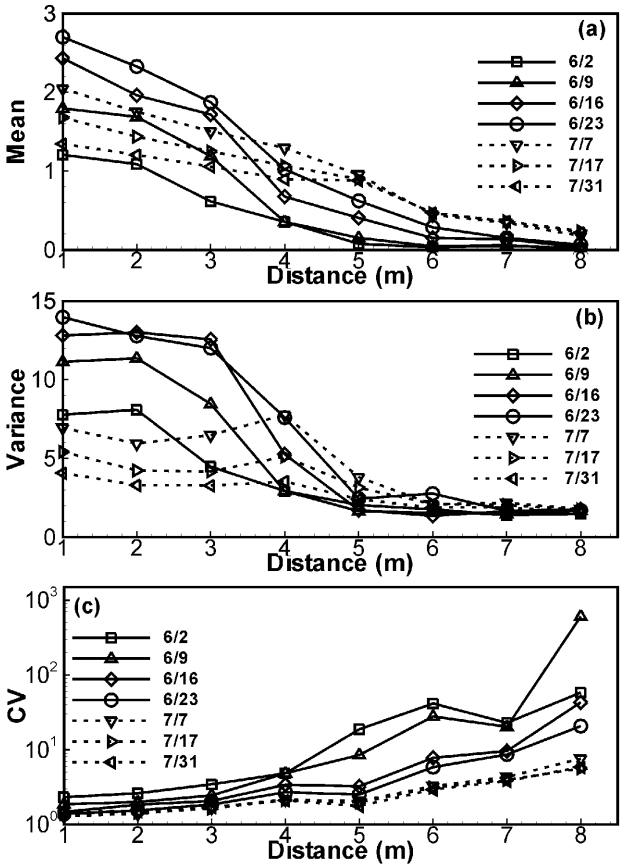

Figure 9. (a) Mean (%), (b) variance (%^{2}), and (c) coefficients of variation (CV) of observed moisture content differences θ_{diff} as a function of the radial distance from the domain center for different observation days.

textured layer and the previously injected water continued its downward movement through the coarse-textured layer until it encountered another layer of fine-textured material. Dipping of the interface at a depth of about 10 m subsequently induces southeastward migration of the water. After 28 June, no more injections were conducted and the uninterrupted redistribution of the moisture plume began. The temporal evolution of the spatial pattern of θ_{diff} unequivocally reveals the effect of media heterogeneities at the site.

[28] Figures 9a, 9b, and 9c illustrate the mean, variance, and CV (i.e., standard deviation/mean), respectively, of the observed θ_{diff} values for various observation days and for varying radial distances from the center of the flow domain. While it is apparent that the mean moisture content increases during the successive injections, the CV generally decreases. For any given observation day, the mean θ decreases with distance while the CV increases. These results support the moisture-dependent variability suggested by the stochastic analysis [*Yeh et al.*, 1985c, equation (2)], i.e., the moisture content variability increases as θ decreases. *Ferrante and Yeh* [1999] showed that the head variance is highest near the wetting front, where the gradient is the largest— an observation similar to stochastic results for concentration plumes [*Gelhar*, 1993]. The mean-distance and variance-distance plots (Figures 9a and 9b) suggesting large changes in the mean θ within the 4 m radius where large θ variances are present appear to support Ferrante and Yeh's results.

5. Spatial Moments of Moisture Plumes

[29] The preceding geostatistical analysis quantifies the change in sills and ranges of the θ plume during the injection experiment. To quantify the migration and spread of the plume at different times, we use the spatial moments of θ differences [*Aris*, 1956]:

$$M_{ijk}(t) = \int_{-\infty}^{+\infty}\int_{-\infty}^{+\infty}\int_{-\infty}^{+\infty} \theta_{diff}(x,y,z,t)x^i y^j z^k dxdydz \qquad (4)$$

The zeroth, first and second spatial moments correspond to $i + j + k = 0$, 1, and 2, respectively. The zeroth moment (M_{000}) represents the changes in moisture storage within the domain. The normalized first spatial moments,

$$x_c = M_{100}/M_{000}, \quad y_c = M_{010}/M_{000}, \quad z_c = M_{001}/M_{000}, \qquad (5)$$

represent the location (x_c, y_c, z_c) of the mass center of the plume at a given time. The spread of the plume about its center is described by the symmetric second spatial variance tensor:

$$\sigma^2 = \begin{bmatrix} \sigma_{xx}^2 & \sigma_{xy}^2 & \sigma_{xz}^2 \\ \sigma_{yx}^2 & \sigma_{yy}^2 & \sigma_{yz}^2 \\ \sigma_{zx}^2 & \sigma_{zy}^2 & \sigma_{zz}^2 \end{bmatrix} \sigma_{xx}^2 = \frac{M_{200}}{M_{000}} - x_c^2 \quad \sigma_{yy}^2 = \frac{M_{020}}{M_{000}} - y_c^2$$
$$\sigma_{zz}^2 = \frac{M_{002}}{M_{000}} - z_c^2$$
$$\sigma_{xy}^2 = \sigma_{yx}^2 = \frac{M_{110}}{M_{000}} - x_c y_c \ \sigma_{xz}^2 = \sigma_{zx}^2 = \frac{M_{101}}{M_{000}} - x_c z_c \ \sigma_{yz}^2 = \sigma_{zy}^2 = \frac{M_{011}}{M_{000}} - y_c z_c. \qquad (6)$$

While moisture plumes with multiple peaks are apparent in Figure 8, a unimodal distribution is assumed in our analysis.

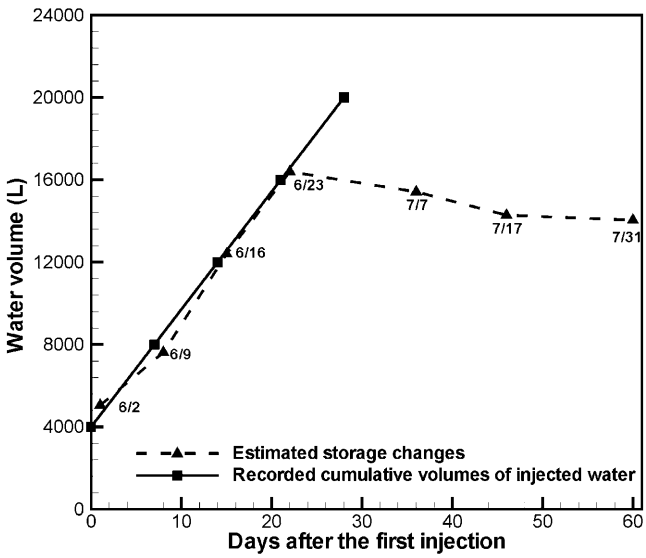

Figure 10. Estimated storage changes and recorded cumulative volumes of injected water versus days after the first injection.

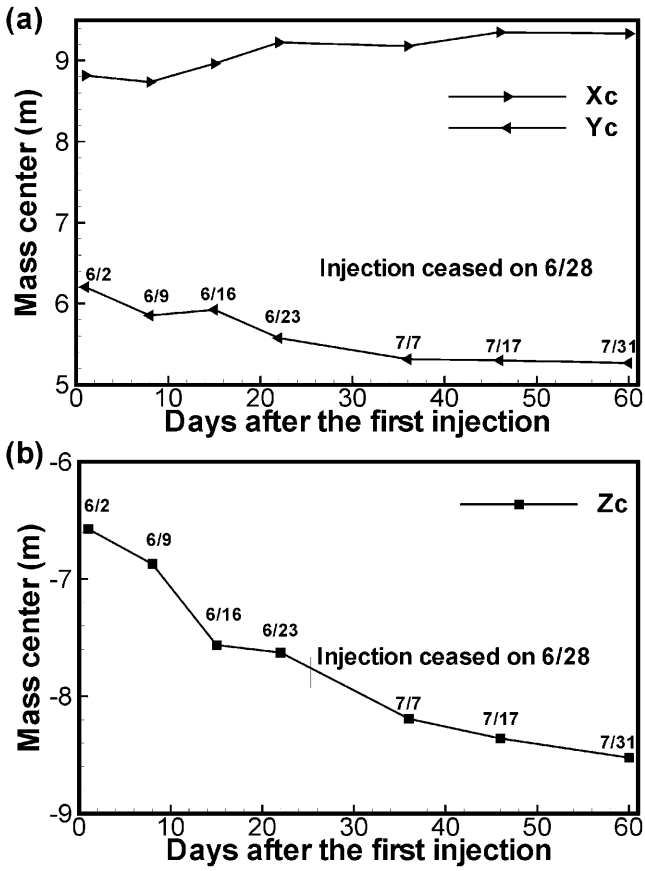

Figure 11. Spatiotemporal evolution of mass center of the moisture plume in (a) x and y and (b) z directions. Vertical axis of Figure 11a is the distance from the bottom left corner of the domain.

This is the same approach used in the analysis of solute plumes at Borden [*Sudicky*, 1986], Cape Cod [*Garabedian et al.*, 1991], and Mississippi [*Adams and Gelhar*, 1992] experiment sites. Hence our analysis results reflect only the overall plume behavior, not the detailed shape of the plume.

[30] Figure 10 shows that before 7 July, the cumulative changes (zero moment) in moisture storage estimated from θ_{diff} agree well with the recorded cumulative injected volume at different times. This suggests that our estimated θ distributions conserve mass. Our calculated moments are on the basis of θ_{diff} and are different from those of *Gee and Ward* [2001], who used θ in their moment calculations. Note that after 7 July, because of lateral migration of the plume beyond the sampling domain (Figures 8f–8h), estimated values are significantly smaller than the cumulative injected volume (20,000 L) recorded on 28 June. Figure 11 illustrates the temporal evolution of the mass center of the θ plume in the x, y, and z directions. Overall, x_c moved eastward, y_c moved southward, and z_c moved downward thus resulting in a southeastward and downward movement of the moisture plume. The trend in the movement of mass centers is similar to that of *Gee and Ward* [2001, Table 4.1] but the values are again different due to their use of θ. Nonetheless, the mass centers moved most rapidly during the early part of the injection experiment. In the z direction, the mass center traveled downward about 1 m for the first 15 days, but about 1.1 m in the following 45 days. In x and y directions, the mass centers traveled less than 1 m over the entire 60 days. After injections ceased (28 June), the mass centers in the x and y directions changed very little.

[31] Figure 12 illustrates the temporal evolution of components of the moisture content spatial variance tensor. The spatial variances (σ^2_{xx}, σ^2_{yy}, and σ^2_{zz}) of the plume increased with time, indicative of the continuous spreading of the plume around its mass center in x, y, and z directions during the injection experiment. The larger spatial variances in the x and y directions than in the z direction suggest greater spreading in the horizontal plane than in the vertical. The cross-covariances (σ^2_{xy}, σ^2_{xz} and σ^2_{yz}) are nonzero because the principal directions of the moisture plume were not aligned with the x-y-z coordinate system. Note that the trace of the calculated second moment tensor (equation (6)) along the principal directions is smaller than that reported by *Gee and Ward* [2001, Table 4.1] because of their use of θ, instead of θ_{diff} for moment calculations. However, as expected, the trend in the magnitude of spreading (Figure 12) for different days is similar to that of *Gee and Ward* [2001, Table 4.1].

[32] The spatial variance tensor was diagonalized by a coordinate transformation. The resultant eigenvectors are principal directions and constitute an orthogonal coordinate system. The eigenvalues are the spatial variance of the moisture plume along the three principal directions. The eigenvalues and eigenvectors facilitate drawing of a 3-D ellipsoid to describe the average shape and orientation of the moisture plume for each observation period. The 3-D ellipsoid is centered at the transformed mass center with semi-axes parallel to the eigenvectors. The semi-axes have

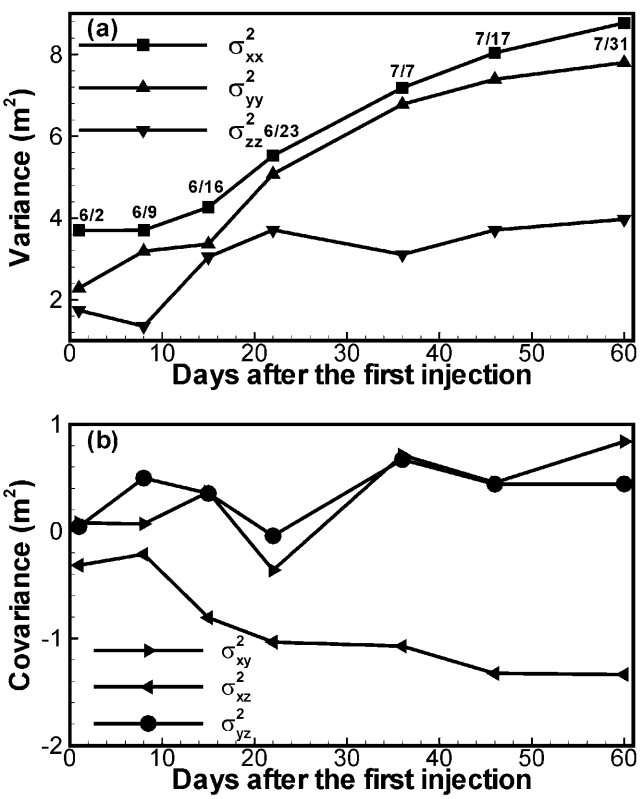

Figure 12. Temporal changes of (a) diagonal and (b) off-diagonal components of the spatial covariance tensor of the moisture plume.

Table 2. Direction Angles Between Eigenvectors of the Second Moment Matrix With x, y, and z Axes of the Original Coordinate System

	α, deg	β, deg	γ, deg
	2 June 2000		
$\mathbf{b}_x$	9.28	87.20	98.84
$\mathbf{b}_y$	80.83	95.30	10.61
$\mathbf{b}_z$	91.93	5.96	84.34
	9 June 2000		
$\mathbf{b}_x$	84.8	104.2	15.1
$\mathbf{b}_y$	91.9	14.5	75.6
$\mathbf{b}_z$	174.5	93.2	85.5
	16 June 2000		
$\mathbf{b}_x$	64.7	116.8	38.4
$\mathbf{b}_y$	85.5	28.1	62.3
$\mathbf{b}_z$	154.2	97.9	65.6
	23 June 2000		
$\mathbf{b}_x$	65.1	84.1	25.7
$\mathbf{b}_y$	76.7	18.4	102.5
$\mathbf{b}_z$	151.3	72.6	67.9
	7 July 2000		
$\mathbf{b}_x$	75.2	101.4	18.9
$\mathbf{b}_y$	118.1	34.0	72.5
$\mathbf{b}_z$	147.6	121.5	83.2
	17 July 2000		
$\mathbf{b}_x$	73.9	97.5	17.9
$\mathbf{b}_y$	104.0	18.4	78.4
$\mathbf{b}_z$	158.4	106.7	76.6
	31 July 2000		
$\mathbf{b}_x$	74.5	98.6	17.8
$\mathbf{b}_y$	111.2	25.8	75.9
$\mathbf{b}_z$	153.3	114.1	79.3

lengths of $l\sigma_p$, where σ_p is the square root of the eigenvalues (p being x, y, or z) and l is a constant. The ellipses in Figure 8 are east-west cross sections (passing through the injection well) of such ellipsoids with $l = 2$. They encompass most of the moisture plume, and represent the spread of the moisture plume in an equivalent homogeneous medium. The longest axes of the ellipses began to orientate downward apparently after 16 June, due to a significant vertical movement of the injected water in the coarse-textured layer. During the uninterrupted redistribution after 7 July, the downward dip of the ellipse was reduced and the ellipses are also elongated southeastward.

[33] Principal directions of the 3-D ellipsoid vary with time; their direction angles are listed in Table 2, where $0° \leq \alpha, \beta, \gamma \leq 180°$ are the angles between eigenvector $\mathbf{b}_p$ (p being x, y, or z) with x, y, and z axes of the original coordinate system of reference, respectively. Figure 13 illustrates the variation for the 3-D ellipsoids on 2 June, 16 June, and 31 July and the associated principal directions. Figures 13a–13c illustrate the change in the shape of the ellipsoids, indicating the increasing dominance of lateral spreading. The southeast movement of the moisture plume is also indicated by Figure 13, recalling that the major axis of the ellipsoid on 31 July is $\mathbf{b}_y$. The dipping angle of $\mathbf{b}_z$ increases during the injection period and decreases during the redistribution period. These observed changes in the principal directions have not been considered in previous stochastic analysis of unsaturated flow and suggest that the principal directions of the effective hydraulic conductivity tensor perhaps vary as the plume evolves.

[34] Figure 14 depicts the relationship between spatial variance ratios, $\sigma_{xx}^2/\sigma_{zz}^2$ and $\sigma_{yy}^2/\sigma_{zz}^2$, and average θ_{diff}, which is the moisture storage change (the zeroth spatial moment) divided by the ellipsoid volume. These ratios are larger than one, implying that spreading in the lateral direction is larger than in the vertical. Furthermore, the ratios vary with average θ differences at different times, indicative of the change in relative importance of lateral spreading and downward movement for the migration of the injected water. These ratios also describe the evolving flow pattern as the injected water migrated and broke through the fine-textured layer into the underlying coarse unit. These ratios, in effect, are a quantitative reflection of the shape and orientation of ellipses shown in Figures 8 and 13, and can be explained on the basis of relative contributions of lateral and vertical migration. Immediately following the first injection on 2 June, the $\sigma_{xx}^2/\sigma_{zz}^2$ ratio is large and becomes even larger on 9 June, following the second injection. Similarly, the $\sigma_{yy}^2/\sigma_{zz}^2$ ratio on 2 June is smaller than that on 9 June. Nonetheless, between 9 and 16 June, the dominance of vertical migration is clearly evident; both ratios become smaller by 16 June. This is consistent with the shape and orientation of the ellipse in Figure 8d. The dominant effect of lateral migration is apparent again following the last injection on 22 June. During redistribu-

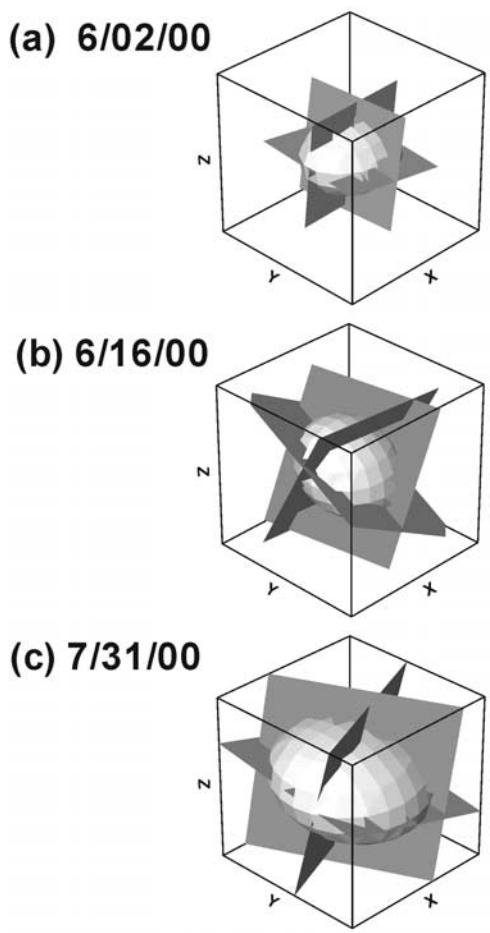

Figure 13. Principal directions of the moisture ellipsoids on (a) 2 June 2000, (b) 16 June 2000, and (c) 31 July 2000.

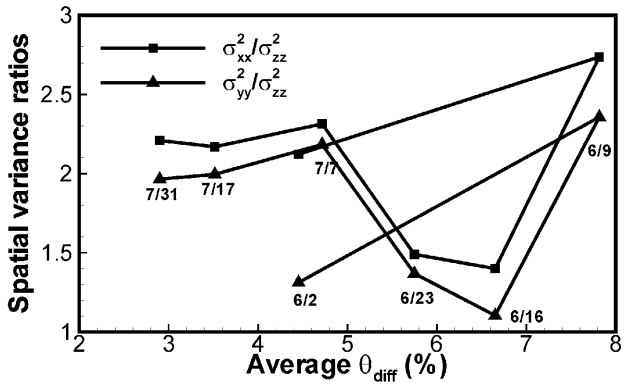

Figure 14. Spatial variance ratio versus average moisture content difference.

tion, both ratios are larger, thus indicating again the predominance of lateral migration. Finally, if the entire domain is assumed to be homogeneous, the relationship between the spatial variance ratio and average θ_{diff} indicates moisture-dependent anisotropy in effective unsaturated hydraulic conductivity [e.g., *Yeh et al.*, 1985a, 1985b, 1985c].

[35] Our results show that the spatial moment analysis is a useful tool for quantifying the bulk movement of the injected water during the experiment. Spatial moments at different times can provide information for estimating effective hydraulic conductivity of the vadose zone and its anisotropy as we demonstrate in the companion paper [*Yeh et al.*, 2005]. Changes in the correlation structure of the moisture plume dynamics suggest the need for considering the evolving correlation structures during unsaturated zone parameter identification procedures [e.g., *Hughson and Yeh*, 2000] or in interpretation of geophysical surveys [e.g., *Yeh et al.*, 2002; *Liu and Yeh*, 2004] and other stochastic analyses of vadose zone hydrologic processes.

6. Concluding Remarks

[36] This study demonstrates that geostatistical and moment analyses are useful tools for quantifying three-dimensional moisture plume dynamics of a field injection experiment. Our geostatistical analysis shows that the initial θ distribution (or geologic heterogeneity) at the S&L site varies, at least, at two scales: (1) lamination structures of large horizontal correlation scales and a vertical correlation scale that is less than 0.305 m within each layer, and (2) the layered structures that are approximately 3.5 m in the vertical and greater than 16 m in the horizontal. Analysis of all the θ data during the injection experiment illustrates the dynamically evolving correlation structures and variances of the moisture plume. These evolving correlation structures have not been reported in previous stochastic analyses of unsaturated flow. Kriged 3-D θ distributions facilitate a better understanding of the impacts of the lithology on the movement of injected water at the field site. The results of stochastic analyses [*Yeh et al.*, 1985a, 1985b, 1985c; *Ferrante and Yeh*, 1999] on steady and transient infiltration are corroborated by the analysis of observed θ differences for different observation days as a function of the radial distance. That is, the moisture content variability is found to increase as the mean θ decreases and large variances occur near locations where high-mean moisture gradients are present.

[37] Spatial moment analyses further quantify the dynamics of moisture movement due to the injection experiment. The first moment shows that the center of the moisture plume moved toward southeast and downward at a faster rate during early times than during late times. The spatial variance tensor suggests that the horizontal spreading is larger than the vertical spreading, and the lateral spreading of the injected water increases as the mean moisture content decreases. This finding appears to support the moisture-dependent anisotropy concept suggested by previous stochastic analyses. However, the principal directions of the moisture plume are found to vary as it migrates, apparently controlled by local geologic structures, instead of spatial statistical structures. Finally, results of this part of the paper lead to the development of a new and practical technique, independent of previous stochastic analyses, for estimating the 3-D effective unsaturated hydraulic conductivity tensor under transient flow conditions. The new technique is presented in the companion paper [*Yeh et al.*, 2005].

[38] **Acknowledgments.** The injection site experiments in the year 2000 were conducted as part of the Vadose Zone Transport Field Study at the Hanford Site; Glendon Gee of Pacific Northwest National Laboratory (PNNL) was the project manager. Anderson Ward of PNNL provided the moisture content data. J. Buck Sisson (formerly of Rockwell Hanford Operations, Richland, WA) originally designed the injection test site layout and conducted the first experiments at the site back in 1980. Alexandre Desbarats provided assistance with the variogram analyses and a very thoughtful and constructive review and suggestions on an earlier version of the manuscript. The work reported was performed for the CH2M Hill Hanford Group Inc. and the U.S. Department of Energy under contract DE-AC06-99RL14047. The third author was funded in part by a NSF/SERDP grant EAR-0229717 and NSF grant IIS-0431079. Reference herein to any specific commercial product, process, or service by trade name, trademark, manufacturer, or otherwise, does not necessarily constitute or imply its endorsement, recommendation, or favoring by the United States Government or any agency thereof or its contractors or subcontractors. The views and opinions of the authors do not necessarily state or reflect those of the United States Government or any agency thereof.

References

Ababou, R. (1988), Three-dimensional flow in random porous media, Ph.D. dissertation, Mass. Inst. of Technol., Cambridge, Mass.

Adams, E. E., and L. W. Gelhar (1992), Field study of dispersion in a heterogeneous aquifer: 2. Spatial moments analysis, *Water Resour. Res.*, *28*, 3293–3307.

Aris, R. (1956), On the dispersion of a solute in a fluid flowing through a tube, *Proc. R. Soc. London, Ser. A*, *235*, 67–78.

Barrash, W., and T. Clemo (2002), Hierarchical geostatistics and multifacies systems: Boise Hydrogeophysical Research Site, Boise, Idaho, *Water Resour. Res.*, *38*(10), 1196, doi:10.1029/2002WR001436.

Crosby, J. W., D. L. Johnstone, C. H. Drake, and R. L. Fenton (1968), Migration of pollutants in a glacial outwash environment, *Water Resour. Res.*, *4*, 1095–1114.

Crosby, J. W., D. L. Johnstone, and R. L. Fenton (1971), Migration of pollutants in a glacial outwash environment: 2, *Water Resour. Res.*, *7*, 204–208.

Deutsch, C. V., and A. G. Journel (1998), *GSLIB—Geostatistical Software Library and User's Guide*, Oxford Univ. Press, New York.

Fayer, M. J., R. E. Lewis, R. E. Engelman, A. L. Pearson, C. J. Murray, J. L. Smoot, R. R. Randall, W. H. Wegener, and A. H. Lu (1995), Re-evaluation of a subsurface injection experiment for testing flow and transport models, *PNL-10860*, Pac. Northwest Natl. Lab., Richland, Wash.

Ferrante, M., and T.-C. J. Yeh (1999), Head and flux variability in heterogeneous unsaturated soils under transient flow conditions, *Water Resour. Res.*, *35*, 1471–1479.

Garabedian, S. P., D. R. LeBlanc, L. W. Gelhar, and M. A. Celia (1991), Large-scale natural gradient tracer test in sand and gravel, Cape Cod, Massachusetts: 2. Analysis of spatial moments for a nonreactive tracer, *Water Resour. Res.*, *27*, 911–924.

Gee, G. W., and A. L. Ward (2001), Vadose zone transport field study: Status report, *PNNL-13679*, Pac. Northwest Natl. Lab., Richland, Wash.

Gelhar, L. W. (1993), *Stochastic Subsurface Hydrology*, 390 pp., Prentice-Hall, Upper Saddle River, N. J.

Gelhar, L. W., A. Mantoglou, C. Welty, and K. R. Rehfeldt (1985), A review of field-scale physical solute transport processes in saturated and unsaturated porous media, *Rep. EA-4190*, Electric Power Res. Inst., Palo Alto, Calif.

Greenholtz, D. E., T.-C. J. Yeh, M. S. B. Nash, and P. J. Wierenga (1988), Spatial variability of soil water tension, soil water content and unsaturated hydraulic conductivity, *J. Contam. Hydrol.*, *3*, 227–250.

Holt, R. M., J. L. Wilson, and R. J. Glass (2002), Spatial bias in field-estimated unsaturated hydraulic properties, *Water Resour. Res.*, *38*(12), 1311, doi:10.1029/2002WR001336.

Hughson, D. L., and T.-C. J. Yeh (2000), An inverse model for three-dimensional flow in variably saturated porous media, *Water Resour. Res.*, *36*, 829–839.

Isaaks, E. H., and R. M. Srivastava (1989), *An Introduction to Applied Geostatistics*, Oxford Univ. Press, New York.

Khaleel, R., and E. J. Freeman (1995), Variability and scaling of hydraulic properties for 200 area soils, Hanford Site, *WHC-EP-0883*, Westinghouse Hanford Co., Richland, Wash.

Khaleel, R., J. F. Relyea, and J. L. Conca (1995), Evaluation of van Genuchten-Mualem relationships to estimate unsaturated conductivity at low water contents, *Water Resour. Res.*, *31*, 2659–2668.

Knoll, K. C., and J. L. Nelson (1962), Radioisotope and moisture distribution beneath a model crib, *HW-71573*, Hanford Atomic Prod. Oper., Richland, Wash.

Last, G. V., and T. G. Caldwell (2001), Core sampling in support of the vadose zone transport field study, *PNNL-13454*, Pac. Northwest Natl. Lab., Richland, Wash.

Last, G. V., T. G. Caldwell, and A. T. Owen (2001), Sampling of boreholes WL-3A through -12 in support of the vadose zone transport field study, *PNNL-13631*, Pac. Northwest Natl. Lab., Richland, Wash.

Liu, S., and T.-C. J. Yeh (2004), An integrative approach for monitoring water movement in the vadose zone, *Vadose Zone J.*, *3*, 681–692.

Lu, A., and R. Khaleel (1993), Calibration/validation of VAM3D model using injection test data at Hanford, in *Vadose Zone Modeling Workshop Proceedings, March 29–30, 1993*, *WHC-MR-0420*, edited by R. Khaleel, Westinghouse Hanford Co., Richland, Wash.

Mantoglou, A., and L. W. Gelhar (1987), Stochastic modeling of large-scale transient unsaturated flow, *Water Resour. Res.*, *23*, 37–46.

Mualem, Y. (1976), A new model for predicting the hydraulic conductivity of unsaturated porous media, *Water Resour. Res.*, *12*, 513–522.

Olgaard, P. L. (1965), On the theory of neutron method for measuring the water content in soil, *Rep. 97*, Dan. At. Energy Comm., Riso.

Palmquist, W. N., and A. I. Johnson (1962), Vadose flow in layered and nonlayered materials, *U.S. Geol. Surv. Prof. Pap.*, *450-C*, 142–143.

Polmann, D. J., D. Mclaughlin, S. Luis, L. W. Gelhar, and R. Ababou (1991), Stochastic modeling of large-scale flow in heterogeneous unsaturated soils, *Water Resour. Res.*, *27*, 1447–1458.

Price, S. M., R. B. Kasper, M. K. Additon, R. M. Smith, and G. V. Last (1979), Distribution of plutonium and americium beneath the 216-Z-1A crib: A status report, *RHO-ST-17*, Rockwell Hanford Oper., Richland, Wash.

Priestley, M. B. (1981), *Spectral Analysis and Time Series*, 890 pp., Elsevier, New York.

Prill, R. C. (1977), Movement of moisture in the unsaturated zone in a loess-mantled area, southwestern Kansas, *U.S. Geol. Surv. Prof. Pap.*, *1021*.

Pyrcz, M. J., and C. V. Deutsch (2003), The whole story on the hole effect, *Newsl. 18*, Geostatistical Association of Australasia, West Perth, West. Aust., Australia.

Rockhold, M. L., C. J. Murray, and M. J. Fayer (1999), Conditional simulation and upscaling of soil hydraulic properties, in *Characterization and Measurement of the Hydraulic Properties of Unsaturated Porous Media*, vol. 2, edited by M. T. van Genuchten, F. J. Leij, and L. Wu, pp. 1391–1401, Univ. of Calif. Press, Riverside.

Routson, R. C., W. H. Price, D. J. Brown, and K. R. Fecht (1979), High level waste leakage from the 241-T-106 tank at Hanford, *RHO-ST-14*, Rockwell Hanford Oper., Richland, Wash.

Rudolph, D. L., R. G. Kachanoski, M. A. Celia, and D. R. LeBlanc (1996), Infiltration and solute transport experiments in unsaturated sand and gravel, Cape Cod, Massachusetts: Experimental design and overview of results, *Water Resour. Res.*, *32*, 519–532.

Sisson, J. B., and A. H. Lu (1984), Field calibration of computer models for application to buried liquid discharges: A status report, *RHO-ST-46P*, Rockwell Hanford Oper., Richland, Wash.

Smoot, J. L. (1995), Development of a geostatistical accuracy assessment approach for modeling water content in unsaturated lithologic units, Ph.D. dissertation, Univ. of Idaho, Moscow.

Sudicky, E. A. (1986), A natural gradient experiment on solute transport in a sand aquifer: Spatial variability of hydraulic conductivity and its role in the dispersion process, *Water Resour. Res.*, *22*, 2069–2082.

Trautwein, S. J., D. E. Daniel, and H. W. Cooper (1983), Case history study of water flow through unsaturated soil, in *The Role of the Unsaturated Zone in Radioactive and Hazardous Waste Disposal*, edited by J. W. Mercer et al., Ann Arbor Sci., Ann Arbor, Mich.

van Genuchten, M. T. (1980), A closed-form solution for predicting the conductivity of unsaturated soils, *Soil Sci. Soc. Am. J.*, *44*, 892–898.

Wackernagel, H. (1995), *Multivariate Geostatistics: An Introduction with Applications*, Springer, New York.

Ward, A. L., T. G. Caldwell, and G. W. Gee (2000), Vadose zone transport field study: Soil water content distributions by neutron moderation, *PNNL-13795*, Pac. Northwest Natl. Lab., Richland, Wash.

Wierenga, P. J., D. B. Hudson, and M. R. Kirkland (1991a), The second Las Cruces trench experiment: Experimental results and two-dimensional flow predictions, *Water Resour. Res.*, *27*, 2707–2718.

Wierenga, P. J., R. G. Hills, and D. B. Hudson (1991b), The Las Cruces trench site: Characterization, experimental results, and one-dimensional flow predictions, *Water Resour. Res.*, *27*, 2695–2705.

Yeh, T.-C. J., L. W. Gelhar, and A. L. Gutjahr (1985a), Stochastic analysis of unsaturated flow in heterogeneous soils: 1. Statistically isotropic media, *Water Resour. Res.*, *21*, 447–456.

Yeh, T.-C. J., L. W. Gelhar, and A. L. Gutjahr (1985b), Stochastic analysis of unsaturated flow in heterogeneous soils: 2. Statistically anisotropic media, *Water Resour., Res.*, *21*, 457–464.

Yeh, T.-C. J., L. W. Gelhar, and A. L. Gutjahr (1985c), Stochastic analysis of unsaturated flow in heterogeneous soils: 3. Observations and applications, *Water Resour. Res.*, *21*, 465–471.

Yeh, T.-C. J., L. W. Gelhar, and P. J. Wierenga (1986), Field observations of spatial variation of soil water pressure in a field soil, *Soil Sci.*, *142*(1), 7–11.

Yeh, T.-C. J., S. Liu, R. J. Glass, K. Baker, J. R. Brainard, D. L. Alumbaugh, and D. LaBrecque (2002), A geostatistically based inverse model for electrical resistivity surveys and its applications to vadose zone hydrology, *Water Resour. Res.*, *38*(12), 1278, doi:10.1029/2001WR001204.

Yeh, T.-C. J., M. Ye, and R. Khaleel (2005), Estimation of effective unsaturated hydraulic conductivity tensor using spatial moment of observed moisture plume, *Water Resour. Res.*, *41*, W03014, doi:10.1029/2004WR003736.

R. Khaleel, Fluor Government Group, P. O. Box 1050, Richland, WA 99352, USA.

M. Ye, Desert Research Institute, University and Community College System of Nevada, 755 E. Flamingo Road, Las Vegas, NV 89119, USA.

T.-C. J. Yeh, Department of Hydrology and Water Resources, University of Arizona, Tucson, AZ 85721, USA. (yeh@hwr.arizona.edu)

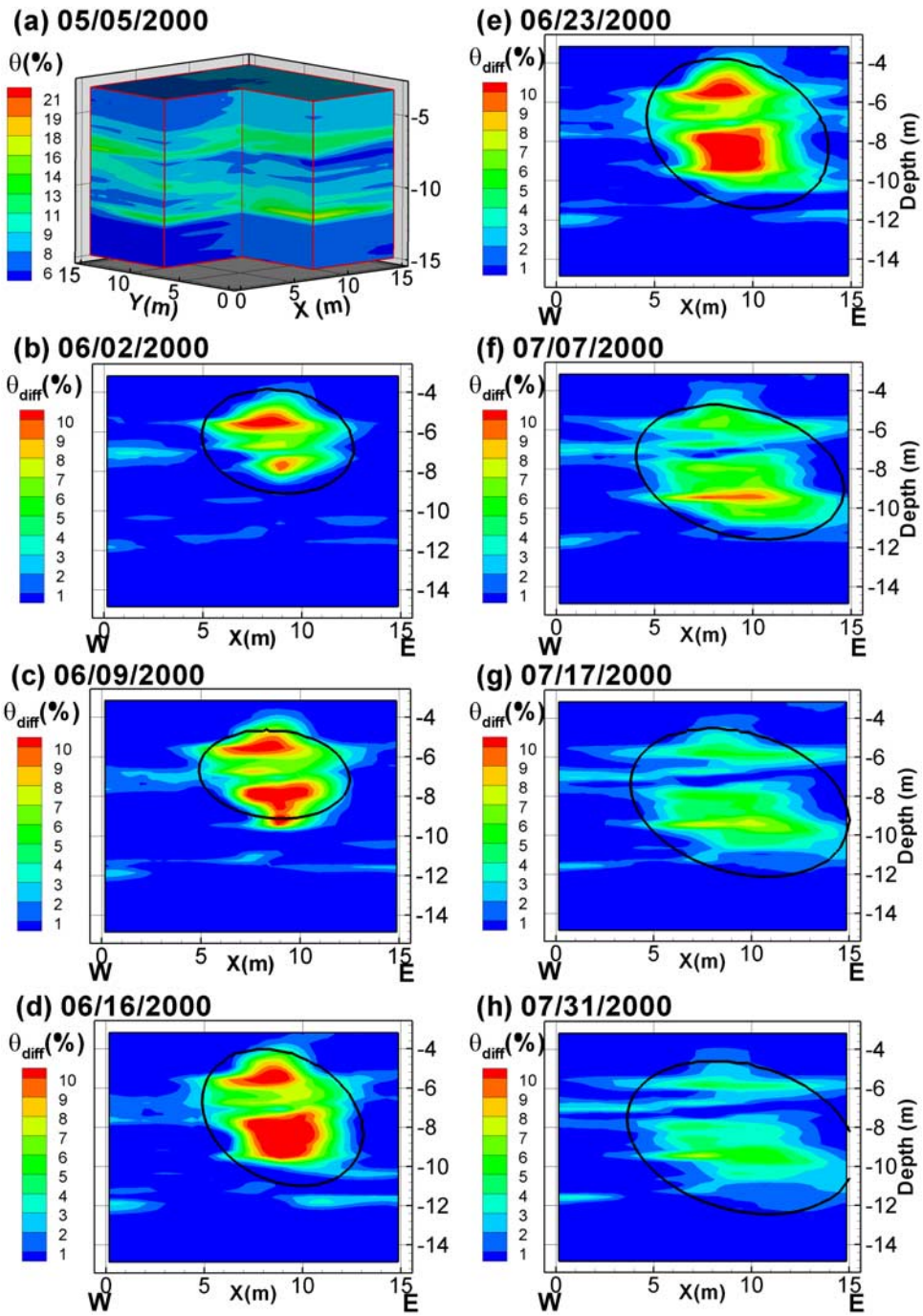

Figure 8. (a) Initial moisture content on 5 May and (b–h) east-west trending cross-sectional views of moisture content differences along the plane passing through the injection well.